OPEN ACCESS
IOP Publishing
Made open access 6 June 2019
Nanotechnology
Nanotechnology **30** (2019) 265401 (8pp)
https://doi.org/10.1088/1361-6528/ab0ecd

Thermal conductivity in disordered porous nanomembranes

Marianna Sledzinska[1], Bartlomiej Graczykowski[2], Francesc Alzina[1], Umberto Melia[3], Konstantinos Termentzidis[4], David Lacroix[5] and Clivia M Sotomayor Torres[1,6]

[1] Catalan Institute of Nanoscience and Nanotechnology (ICN2), CSIC and The Barcelona Institute of Science and Technology Campus UAB, Bellaterra, E-08193 Barcelona, Spain
[2] Max Planck Institute for Polymer Research, Ackermannweg 10, D-55218 Mainz, Germany
[3] Department of ESAII, Centre for Biomedical Engineering Research, Universitat Politècnica de Catalunya, CIBER-BBN, Barcelona, Spain
[4] Univ Lyon, CNRS, INSA-Lyon, Université Claude Bernard Lyon 1, CETHIL UMR5008, F-69621, Villeurbanne, France
[5] Université de Lorraine, CNRS, LEMTA, Nancy, F-54000, France
[6] ICREA-Institucio Catalana de Recerca i Estudis Avancats, E-08010 Barcelona, Spain

E-mail: marianna.sledzinska@icn2.cat

Received 30 October 2018, revised 27 February 2019
Accepted for publication 12 March 2019
Published 12 April 2019

Abstract

In this work we study the effects of disorder on the thermal conductivity of porous 100 nm thick silicon membranes, in which the size, shape and position of the pores were varied randomly. Measurements using two-laser Raman thermometry on both non-patterned and porous membranes revealed more than a 10-fold reduction of the thermal conductivity compared to that of bulk silicon and a six-fold reduction compared to non-patterned membranes for the sample with random pore shapes. Using Monte Carlo methods we solved the Boltzmann transport equation for phonons and compared different possibilities of pore organization and its influence on the thermal conductivity of the samples. The simulations confirmed that the strongest reduction of thermal conductivity is achieved for a distribution of pores with arbitrary shapes that partially overlap. Up to a 15% reduction of the thermal conductivity with respect to the purely circular pores was predicted for a porous membrane with 37% filling fraction. The effect of the pore shape and distribution was further studied. Maps of temperature and heat flux distributions clearly showed that for particular pore placement heat transport can be efficiently blocked and hot spots can be found in narrow channels between pores. These findings have an impact on the fabrication of membrane-based thermoelectric devices, where low thermal conductivity is required. This work shows that for porous membranes with a given filling fraction the thermal conductivity can be further modified by introducing disorder in the shape and placement of the pores.

Supplementary material for this article is available online

Keywords: silicon nanomembrane, thermal conductivity, Monte Carlo methods, disorder

1. Introduction

Although physical models prefer to describe perfectly ordered systems, they are hard to find in nature; real systems always contain defects and disorder. In many systems the presence of disorder is considered unfavorable, however recent works have shown that it can improve or add functionality to the system. For instance, disordered nanostructures on the surface of flower petals produce visual signals which attract bees [1]. In photonics, photon transport and collimation can be strongly enhanced in disordered structures [2]. Therefore, instead of trying to eliminate disorder in nano-devices in this work we

intentionally introduce disorder during the fabrication process in order to study its effects in nanostructures and obtain new functionalities.

Two-dimensional phononic crystals (PnCs) are periodically patterned membranes and in such structures disorder is mainly discussed in context of phonon coherence and its implication on thermal transport. In a porous material thermal conductivity is influenced by several factors such as porosity, pore size and shape, temperature and the emissivity in the pore [3]. Low thermal conductivity of nanopatterned silicon makes it a potential building block for future thermoelectric devices. We have previously investigated the influence of short-range disorder in Si membrane-based two-dimensional PnCs on their GHz and THz phononic properties and showed that although low-frequency phonon modes are affected by periodicity, their impact is not sufficient to affect thermal conductivity at room temperature (RT). For samples with a period of 300 nm we observed purely diffusive thermal transport and obtained the same value for the thermal conductivity for ordered and disordered PnCs [4].

When the pore and pitch sizes are in the order of few hundreds of nanometers, the position of each pore has been reported to be relevant at very low temperatures. Zen *et al* showed coherent reduction of thermal conductance at sub-Kelvin temperatures [5]. Maire *et al* demonstrated the transition from coherent to purely diffusive heat conduction at 10 K [6]. In a paper by Anufriev *et al* the effect of disorder in circular pore PnCs was further studied. In the later study the disorder induced a reduction of the thermal conductivity at RT and was only measurable in the samples with high filling fraction and periodicity below 200 nm [7].

In this work we studied two samples in which we did not only vary the position of the pores and filling fraction, but also the size and shape distribution of the pores. Detailed sample characterization was performed using scanning electron microscopy (SEM). The thermal conductivity of the samples was measured using two-laser Raman thermometry (2LRT) and the results were compared with Monte Carlo (MC) simulations of phonon transport in similarly disordered membranes.

2. Results

2.1. Samples

Disordered porous membranes can be fabricated using variety of techniques, such as nanocrystallisation, block-copolymer lithography or porous alumina templates. In order to fabricate the disordered structures here we have modified the fabrication process based on electron beam lithography (EBL) and reactive ion etching (RIE) on free-standing membranes (Norcada Inc.) [8]. EBL systems are designed to be robust to external noise in order to reproduce the design with the highest accuracy with reduced shot-noise influence [9]. To intentionally introduce disorder in our structures, we utilized a noise-assisted EBL, where strong external vibrations distort the beam path. As such, a perfectly periodic targeted design of nanoholes (similar to the ones reported previously [10]), became a randomized lattice of deformed holes.

The two structures, hereinafter referred as Sample 1 and Sample 2, fabricated in a membrane of thickness $t = 100$ nm, are shown in figures 1(a) and (b) respectively. The samples were imaged using SEM and images were further analyzed using MATLAB software (supplementary information is available online at stacks.iop.org/NANO/30/265401/mmedia). The effective filling fraction was calculated for Samples 1 and 2 to be of 25% and 37%, respectively. The shapes of the pores were not cylindrical, therefore we computed the distribution of the areas of the pores. Due to the computational reasons, in the MC model we assumed a circular distribution of the pores whilst maintaining the filling fraction and the area distribution of the samples, as shown in figures 1(c) and (d). The comparison between cumulative sum of the areas of the pores obtained experimentally and used in the simulations is shown in figures 1(e) and (f). The insets in figure 1 display the distribution of the pores' diameters assuming a circular shape.

2.2. Two-laser Raman thermometry

Thermal conductivity measurements were performed using 2LRT, which has been successfully applied to 2D free-standing plain [11, 12] and porous membranes [4, 10]. The technique, shown schematically in figure 2(a), consists of using two lasers, one of which (405 nm) is a localized steady-state heat source, while the second laser (532 nm) measures temperature profile utilizing the temperature-dependent frequency of optical phonons [11]. In the case of silicon we use the longitudinal optical phonon mode position (521 cm^{-1} at RT) as a calibrated temperature probe. The position of the mode depends on the temperature with -43.43 ± 0.05 K$(cm^{-1})^{-1}$.

In the experimental set-up both lasers were focused on the samples using 50 × microscope objectives with numerical apertures of NA = 0.55. Both samples had a non-patterned 5 × 5 μm^2 square in the center (figure 1(b)) where the heating laser was focused. Finally, the absorbed power P_{abs} was measured *in situ* for each sample as the difference between the incident light and the sum of transmitted and reflected light intensities by a calibrated system based on a non-polarizing cube beam splitter. All the measurements were performed in a vacuum of 5×10^{-3} mbar.

In order to calculate thermal conductivity of the membranes we need to solve the Fourier heat equation. Due to the small thickness of the membranes we can use the 2D solution for a thermally isotropic medium in steady-state:

$$k = -\frac{P_{abs}}{2\pi t \frac{dT}{d(\ln(r))}}, \quad (1)$$

where r is the distance from the heating spot, t is the membrane thickness, k is the thermal conductivity and T is the temperature.

The non-patterned silicon membrane with $t = 100$ nm was measured as a reference sample. The temperature profile at the absorbed power of $P_{abs} = 2.18$ mW is shown in figure 2(b). The heating laser is placed at $r = 0$, where the

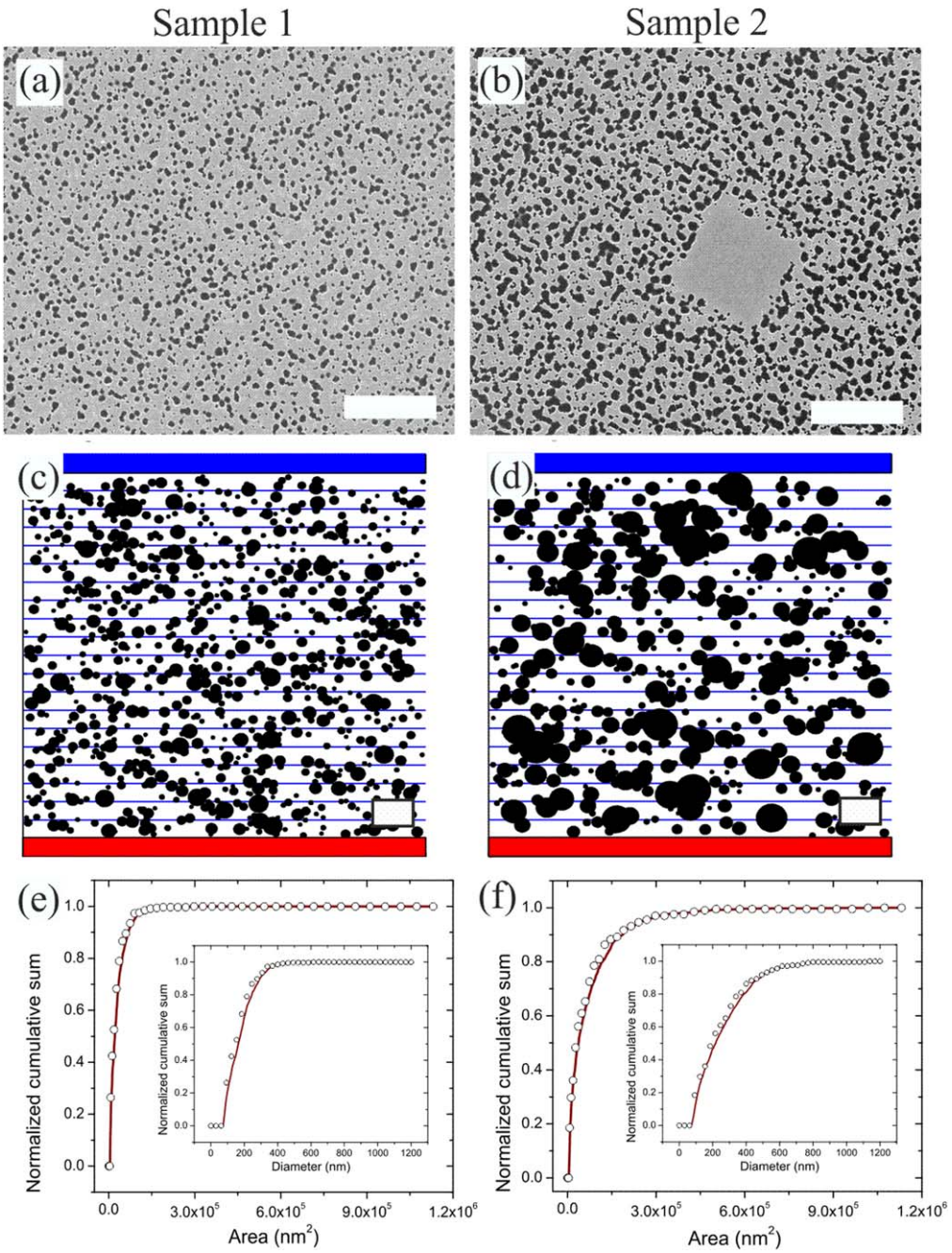

Figure 1. SEM images of (a) Sample 1 with 25% filling fraction and (b) Sample 2 with 37% filling fraction and the detail of the heating island located in the center of the sample. Scale bar 5 μm. Theoretical samples used for MC simulations corresponding to (c) Sample 1 and (d) Sample 2. Red and blue bars correspond to the hot and cold side of the sample, respectively. Scale bar 1 μm. Normalized cumulative sum of the areas of the pores in (e) Samples 1, (f) Sample 2; circles correspond the experimentally measured distributions from SEM, red curves are the modeled distributions derived from figures (c) and (d). Insets correspond to the cumulative sum of the diameters, assuming circular pores for a given area distribution.

temperature increase is the highest and the temperature decay is probed between -500 and 500 μm from the center. The shaded parts are taken into consideration as we are interested in thermal conductivity near RT. Weak temperature dependence of k enables a straightforward procedure for its experimental evaluation. Following equation (1), k can be determined from the slope of $T(\ln(r))$. The solid line in figure 2(c) is the $T(\ln(r))$ linear fit of the experimental data (black circles) from which we obtained $k = 60 \pm 3$ Wm^{-1}K^{-1}. This represents more than a two-fold reduction compared to bulk silicon at RT [13].

Secondly, the two porous samples were measured. The temperature profiles for Samples 1 and 2 are shown in figures 2(d) and (f), respectively, for a given P_{abs}. The extracted values of the intrinsic thermal conductivity taking into account the porosity for these samples were 19 ± 3 and 11 ± 3 Wm^{-1}K^{-1} for the Sample 1 and 2, respectively (figures 2(e) and (g)). This means that thermal conductivity in

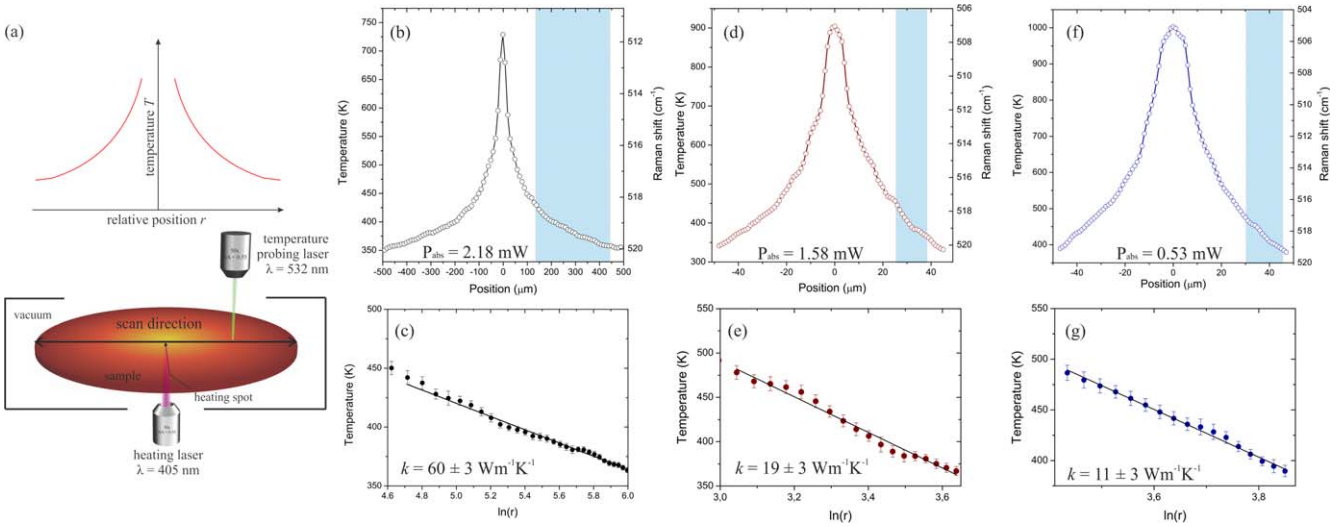

Figure 2. (a) Schematic of the two-laser Raman thermometry set-up and an example of a temperature profile of the sample. Temperature profiles and temperatures as a function of ln(r) for: (b), (c) non-patterned, 100 nm thick membrane. (d), (e) Disordered porous membranes with filling fraction of 25%. (f), (g) Disordered porous membranes with filling fraction of 37%.

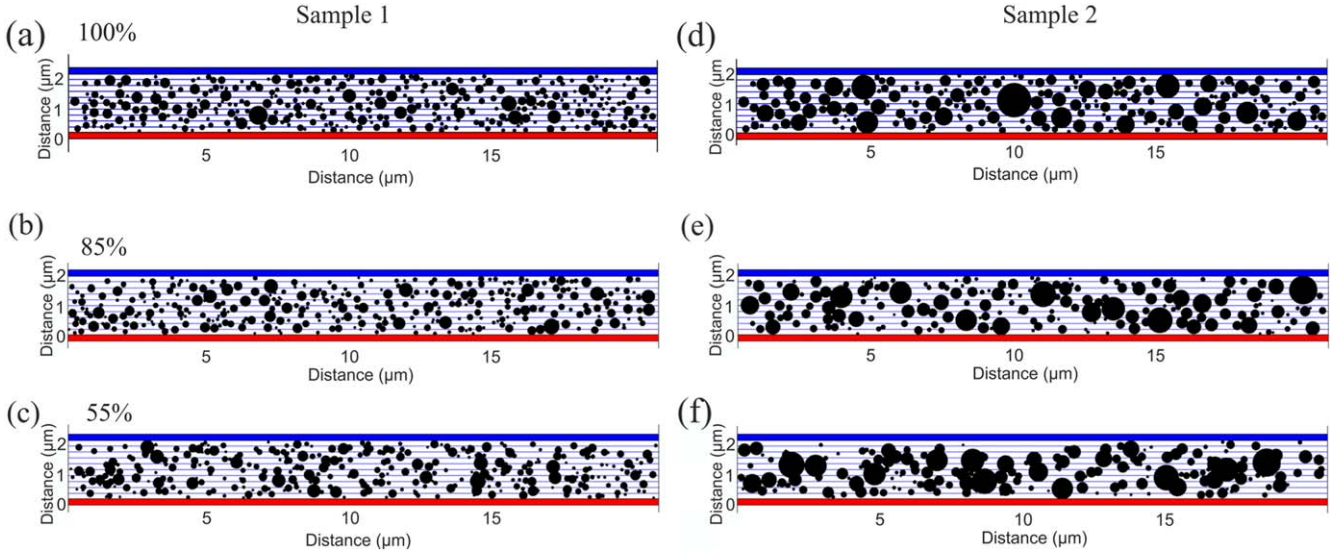

Figure 3. Pore distribution used in Monte Carlo simulations. Sample 1: (a) no overlap (100%), (b) 85% possible overlap (c) 55% possible overlap. Sample 2: (d) no overlap, (e) 85% possible overlap (f) 55% possible overlap. Red and blue rectangular represent the hot and the cold thermostats respectively.

the disordered porous membrane configuration is lowered by one order of magnitude as compared to bulk silicon at RT.

3. Monte Carlo simulations

The Boltzman transport equation (BTE) can be handled with different techniques, particularly those developed around time and space discretization (finite volumes, finite elements, etc) and which are efficient for simple geometries. Creating a mesh for membranes with a disordered distribution of pore size and location is challenging and make finite difference techniques very complex to use. In such a complex geometrical configuration, a MC technique based on energy carrier displacement and scattering is more appropriate and has already proven to be very efficient and reliable. The MC solution of BTE used in this study is derived from a previously developed simulation tool that allows the modeling of plain membranes [14] and porous membranes [15]. In the latter work, mono-dispersed spherical pores or aligned/staggered cylindrical pores were considered. The main evolution of the MC tool in the present work was to make possible the modeling of poly-dispersed cylindrical pores which are allowed to overlap, mimicking the disordered porous membranes achieved experimentally (figure 3). All the basics of phonon transport in nanostructures (drift and scattering of carriers) with the MC method can be found in the previously cited papers. Concerning physical inputs, the dispersion properties of bulk silicon, assuming isotropic dispersion relations, were used. Similarly, phonon lifetimes were derived

Table 1. Summary of the Monte Carlo and experimental results for the cases of varying possible overlap percentage of the pores, resembling sample 1 and sample 2.

	Sample 1		Sample 2		
	k ($Wm^{-1}K^{-1}$)	Porosity (%)	k ($Wm^{-1}K^{-1}$)	Porosity (%)	Overlapping (%)
MC (300 K)	59.3 ± 1.3	0	59.3 ± 1.3	0	—
MC	35.6 ± 0.1	25	30 ± 0.1	37	No
MC	33.1 ± 0.5	26.5	27.4 ± 0.1	38.1	85
MC	32.9 ± 0.1	25.5	27.5 ± 0.2	38	70
MC	32.9 ± 0.1	25.5	25.7 ± 0.6	38	55
MC	33.4 ± 0.1	25.1	27 ± 0.6	36.5	40
MC (400 K)	24.6 ± 0.1	25.5	20.7 ± 0.15	38	55
MC (450 K)	21.9 ± 0.1	25.5	18.5 ± 0.15	38.5	55
Experiment	60 ± 3	0	60 ± 3	0	—
Experiment	19 ± 3	25	11 ± 3	37	—

from bulk according to the Holland formalism [16]. The membrane thickness is taken to be 100 nm (as in the experiment) and random distributions of holes for a porosity of 25% and 37% with overlapping and non-overlapping of holes was studied. Diffuse reflections are assumed from pore boundaries and membrane's surfaces. The width of the samples was varied from 10 to 40 μm and length of the porous part was set to 2 μm, as shown in figure 3. The temperatures set at the hot and cold end were 302 K and 298 K, respectively. In order to reduce the uncertainty, the results were averaged over 16 different membrane configurations for each porosity and overlapping parameters.

First of all, thermal conductivity of a plain 100 nm thick membrane was calculated to be 59.3 ± 1.3 $Wm^{-1}K^{-1}$, in good agreement with the value obtained experimentally. Then we proceed to calculate the thermal conductivity of the porous membranes, assuming circular shape of the pores (non-overlapping) and same filling fractions as the experimental samples. The results obtained for samples 1 and 2, at RT, are of 35 and 30 $Wm^{-1}K^{-1}$, respectively.

4. Discussion

To the best of our knowledge, there is only one paper dealing with disordered porous membranes with similar geometric parameters. In the work by Wolf *et al* numerical simulations were carried out on porous thin films with thickness of 100 nm and pore diameter of 50 nm, with different pore roughness (from diffuse to specular), and random pore locations in the nanostructure [17]. Among the different outputs of the work by Wolf *et al* three main conclusions were drawn. Firstly, increasing porosity leads to thermal conductivity reduction: a three-fold reduction was calculated from unpatterned to 35% porosity. This has been observed in several studies dealing with nanoporous materials, and the results are in the same range as that of those in our work [6, 7, 18]. Secondly, increasing pore roughness, assuming that pores diffusely scatter phonons, also reduces the thermal conductivity; this is also observed in our simulation with a limited impact upon increasing porosity. Once again, this is expected as large porosity makes the overall behavior of the structure diffuse regarding the phonon transport and increasing this diffuse behavior by pore scattering does not affect the calculations. Lastly, the impact of pore placement in the membrane, meaning either a uniform or a non-uniform distribution on the resulting thermal conductivity was studied. This is undoubtedly the most complicated issue to deal with, as it can change the value of the thermal conductivity drastically, up to an order of magnitude depending on the pore spatial distribution. Two extreme cases were applied: the pore can be uniformly located and therefore thermal transport is only ruled by the porosity and specularity at pore interface, or pores can be non-uniformly placed and locally increase the resistance to phonon transport due to the fact that some areas of the membrane have increased apparent porosity. The effect of the pore placement will be further discussed in this section.

Apart from the pore placement, it was previously reported that different shapes of pores (circular, square and triangular) would give varying thermal conductivity, however these simulations were made for pores of a significantly smaller size of about a few nanometers [19]. In the case of a disordered lattice of square pores the k values were 30% lower than that of their aligned counterparts [20]. Therefore, from MC simulations reported previously there is a clear connection between the position/shape of the pores and the thermal conductivity.

In our work, the main difference between the experimental samples and the modeled samples is the shape of the pores. While in the model we assume a circular shape for computational simplicity, the actual shape of the pores in the fabricated sample is undefined. In order to partly reproduce this randomness in form, holes were allowed to overlap, whilst maintaining the filling fraction constant (figures 1(c) and (d)). Overlapping is introduced by weakening the limitation introduced in the previous simulations that the minimal distance between pores is defined when their edges touch, i.e. the center-to-center distance is equal to $R_i + R_j$ where R_i and R_j are the pore radii. This distance was instead varied between 40% and 85% of the previously set limit of $R_i + R_j$ (figure 3). The results for different percentage of allowed overlapping are summarized in table 1. For sample 1 there is a slight

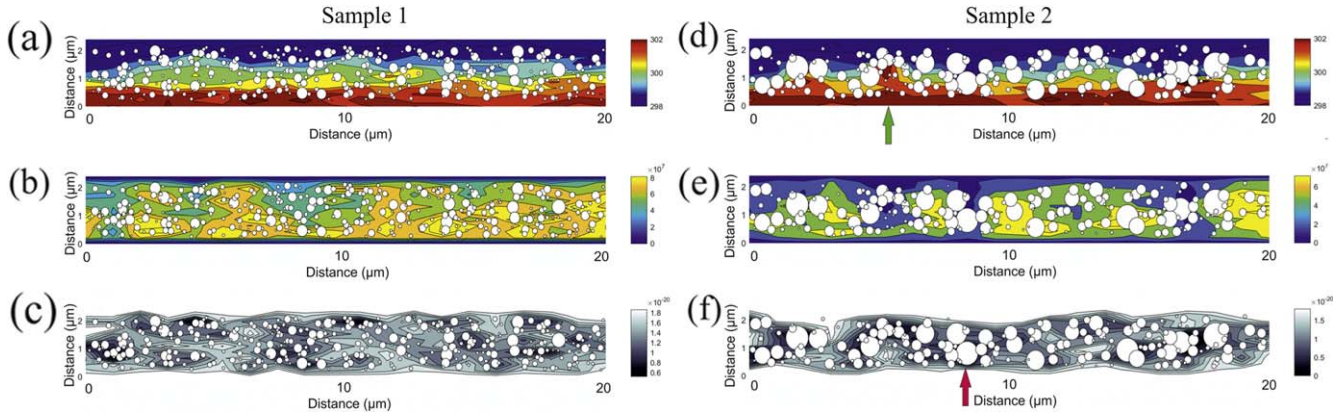

Figure 4. Simulated map of (a)/(d) temperature distribution, (b)/(e) heat flux and (c)/(f) volume distribution (white area present no porosity, while dark area are representative of high porosity) in Sample 1/Sample 2, assuming 55% of hole overlap. The white circles correspond to the overlapping pores present in the samples.

decrease of about 2 $Wm^{-1}K^{-1}$ in thermal conductivity for a 55% of overlapping. More significant results are obtained for sample 2. In this case we obtained a decrease of 4.5 $Wm^{-1}K^{-1}$ for 55% overlapping. In both simulated samples, k is seen to reach a minimal value at 55% of overlapping, and increases with a further decrease of the center-to-center distance. This seems to be related to the optimal value for overlapping giving maximum blocking of the direct paths of heat flow.

We have further studied the influence of the pore placement on the heat transport in porous membranes. For this we calculated maps of temperature and heat flux for Samples 1 and 2, assuming the 55% hole overlap configuration. The simulation domain is of 2.4 μm by 20 μm which is important for nanoscale heat transport calculations, even for MC simulations. In this domain we have considered a discretization of 12 by 20 cells as a reasonable ratio between spatial resolution and the number of sampled phonons (between 30 000 and 60 000 distinct energy bundles) which have to be followed during all the simulation time steps (typically 250 000 time steps of 1 ps).

In figures 4(a) and (d) the temperature distributions are shown. For both samples the temperature is not homogenous within the sample. The same applies to the heat fluxes, shown in figures 4(b) and (e). Instead, both temperature and heat flux depend on the position in the sample. In figures S4 and S5 in supplementary information we show the cross sections of the temperature and heat flux maps in different points of the samples.

Both temperature and heat flux are related to the map of density, shown in figure 4 (c) and (f). In the low density regions (i.e. regions where more holes are present) the heat flow is efficiently blocked and the resulting temperature from linear variation between hot and cold thermostats. At such locations, we can even see 'hot spots' (green arrow in figure 4 (d)). The regions with low density can be understood as a phonon bottlenecks. A phonon bottleneck has been defined as a set of pores representing the highest local resistance to phonon transport [20]. This is more visible for Sample 2, due to its higher porosity. Another example of a phonon bottleneck is marked with red arrow in figure 4 (f). In that region, constituted of various holes either overlapping or placed close to each other, it can be seen that the heat flux is almost zero. This effect is robust in temperature. We have performed the simulations at 200, 300 and 400 K and for all three temperatures we can see the same phonon blocking behavior (see supplementary information).

The effect of phonon bottlenecks on thermal transport has also been recently discussed by Romano *et al* [20]. Even though the simulations were performed for much smaller structures (periods of 10 nm) the results were similar to the ones shown here. The formation of high-flux heat regions is irregular as it depends on the pore configuration and the density of pores along the heat flux direction has a significant influence on thermal conductivity. The disordered circular crystals were found to have average thermal conductivity values of up to 15% lower than that of their aligned counterparts. This is in line with what was observed in our samples, where some parts of the membrane exhibit higher pore density than others. This naturally affects the resulting k both in experimental and MC simulations.

We have calculated the temperature dependence of the thermal conductivity of porous samples with 55% overlap in the range of 250–500 K (see figures S8 in supplementary information). For these simulations the temperature gradient remains equal to 4 K, i.e. $\pm$2 K around the average temperature of the thin film. As expected thermal conductivity decreases accordingly to the evolution of the phonon population and the scattering processes, mostly Umklapp processes, as temperature increases. As the experimental results are an average of the points taken in the range of temperatures between the 500 and 350 K, we can compare them with the simulated results at 400 K, which are 24.6 ± 0.1 and 20.7 ± 0.15 $Wm^{-1}K^{-1}$, and 450 K, which are 21.9 ± 0.1 and 18.5 ± 0.15 $Wm^{-1}K^{-1}$, for samples with 25% and 37% porosity, respectively. These values are in reasonable agreement with the experimental results. The possible reasons for

the small differences in the experimental and calculated values are discussed in the further section.

One effect, which accounts for the lower k of experimental samples, is the roughness and the possible native oxides at the edges of the pores. We have estimated that the roughness for samples fabricated using EBL and RIE to be below 5 nm [4]. However, it is more pronounced in the samples reported in this work, being approximately 7 nm. This roughness comes from the particular fabrication process applied here. It would be logical to assume that this layer inside the pores has lower thermal conductivity than the crystalline silicon of the membrane. Verdier *et al* have showed that amorphous layers on the pores' surface can drastically reduce the overall thermal conductivity of the system [21]. They affect thermal transport through possible localized modes that do not contribute to the energy transport in the material. Therefore we believe that the partly amorphous layer adds to the overall low thermal conductivity.

Finally, from the SEM images we also note that there is a non-negligible amount of small pores (approx. 50 nm diameter) which are not fully etched-through the whole thickness of the membrane (figures A1). They were not taken into account while calculating the filling fraction, but they contribute to the partial reduction of the thermal conductivity, as their phonon scattering efficiency is larger than big pores.

5. Conclusions

In this work we studied two disordered samples with filling fractions of 25% and 37%, for which we measured the thermal conductivity to be 19 ± 3 $Wm^{-1}K^{-1}$ and 11 ± 3 $Wm^{-1}K^{-1}$, respectively. Using MC simulations we have shown that by introducing disorder not only in the location, but also in the shape of the pores we can effectively reduce thermal conductivity. This effect is more pronounced for samples with high filling fraction. According to the simulations, for the sample with 37% filling fraction a decrease in thermal conductivity of approximately 15% can be achieved by introducing 55% of overlap between the pores. Using MC simulations we have also calculated distributions of temperature and heat flux for disordered samples with 55% hole overlap. In these samples both heat flux and temperature do not have a uniform distribution. From the simulations we could identify the particular regions which efficiently block heat transport. This further supports the statement that we can tune the heat transport by different pore arrangements.

We have shown using numerical methods, that for a given porosity of the sample, we can vary the thermal conductivity by varying the position and shape of the pores. This could have an important impact on the fabrication of porous membranes for thermoelectric applications. We have also discussed other possible factors which can influence the thermal conductivity of the experimental samples, such as roughness and the presence of not fully etched-through pores.

Acknowledgments

The ICN2 is funded by the CERCA program/Generalitat de Catalunya. ICN2 is supported by the Severo Ochoa program from Spanish MINECO (Grant No. SEV-2017-0706). We acknowledge the financial support from the Spanish MINECO project PHENTOM (FIS2015-70862-P). We acknowledge the financial support from the French ANR with the project MESOPHON (ANR-15-CE30-0019). BG acknowledges the support from the Foundation for Polish Science (Homing/2016-1/2 and First Team POIR.04.04.00-00-5D1B/18-00) and ERC AdG SmartPhon (Grant No. 694977).

ORCID iDs

Marianna Sledzinska https://orcid.org/0000-0001-8592-1121
Bartlomiej Graczykowski https://orcid.org/0000-0003-4787-8622
Francesc Alzina https://orcid.org/0000-0002-7082-0624
Umberto Melia https://orcid.org/0000-0003-3033-0505
Konstantinos Termentzidis https://orcid.org/0000-0002-8521-7107
David Lacroix https://orcid.org/0000-0001-6067-8524
Clivia M Sotomayor Torres https://orcid.org/0000-0001-9986-2716

References

[1] Moyroud E *et al* 2017 Disorder in convergent floral nanostructures enhances signalling to bees *Nature* **550** 469–74
[2] Hsieh P, Chung C, McMillan J F, Tsai M, Lu M, Panoiu N C and Wong C W 2015 Photon transport enhanced by transverse anderson localization in disordered superlattices *Nat. Phys.* **11** 268
[3] Sugawara A and Yoshizawa Y 1962 An experimental investigation on the thermal conductivity of consolidated porous materials *J. Appl. Phys.* **33** 3135–8
[4] Wagner M R, Graczykowski B, Reparaz J S, El Sachat A, Sledzinska M, Alzina F and Sotomayor Torres C M 2016 Two-dimensional phononic crystals: disorder matters *Nano Lett.* **16** 5661–8
[5] Zen N, Puurtinen T A, Isotalo T J, Chaudhuri S and Maasilta I J 2014 Engineering thermal conductance using a two-dimensional phononic crystal *Nat. Commun.* **5** 3435
[6] Maire J, Anufriev R, Yanagisawa R, Ramiere A, Volz S and Nomura M 2017 Heat conduction tuning by wave nature of phonons *Sci. Adv.* **3** e1700027
[7] Anufriev R, Ramiere A, Maire J and Nomura M 2017 Heat guiding and focusing using ballistic phonon transport in phononic nanostructures *Nat. Commun.* **8** 15505
[8] Sledzinska M, Graczykowski B, Alzina F, Santiso Lopez J and Sotomayor Torres C M 2016 Fabrication of phononic crystals on free-standing silicon membranes *Microelectron. Eng.* **149** 41–5
[9] Kruit P and Steenbrink S W H K 2006 Shot noise in electron-beam lithography and line-width measurements *Scanning* **28** 20–6

[10] Graczykowski B *et al* 2017 Thermal conductivity and air-mediated losses in periodic porous silicon membranes at high temperatures *Nat. Commun.* **8** 415
[11] Reparaz J S, Chavez-Angel E, Wagner M R, Graczykowski B, Gomis-Bresco J, Alzina F and Sotomayor Torres C M 2014 A novel contactless technique for thermal field mapping and thermal conductivity determination: two-laser raman thermometry *Rev. Sci. Instrum.* **85** 034901
[12] Sledzinska M *et al* 2016 Thermal conductivity of MoS_2 polycrystalline nanomembranes *2D Mater.* **3** 035016–22
[13] Maycock P D 1967 Thermal conductivity of silicon, germanium, III–V compounds and III–V alloys *Solid·State Electron.* **10** 161–8
[14] Lacroix D, Joulain K and Lemonnier D 2005 Monte Carlo transient phonon transport in silicon and germanium at nanoscales *Phys. Rev.* B **72** 064305
[15] Jean V, Fumeron S, Termentzidis K, Tutashkonko S and Lacroix D 2014 Monte Carlo simulations of phonon transport in nanoporous silicon and germanium *J. Appl. Phys.* **115** 024304
[16] Holland M G 1964 Phonon scattering in semiconductors from thermal conductivity studies *Phys. Rev.* **134** A471–80
[17] Wolf S, Neophytou N and Kosina H 2014 Thermal conductivity of silicon nanomeshes: effects of porosity and roughness *J. Appl. Phys.* **115** 204306
[18] Anufriev R, Maire J and Nomura M 2016 Reduction of thermal conductivity by surface scattering of phonons in periodic silicon nanostructures *Phys. Rev.* B **93** 045411
[19] Romano G and Grossman J C 2014 Toward phonon-boundary engineering in nanoporous materials *Appl. Phys. Lett.* **105** 033116
[20] Romano G and Grossman J C 2017 Phonon bottleneck identification in disordered nanoporous materials *Phys. Rev.* B **96** 115425
[21] Verdier M, Termentzidis K and Lacroix D 2016 Crystalline-amorphous silicon nano-composites: nano-pores and nano-inclusions impact on the thermal conductivity *J. Appl. Phys.* **119** 175104